Investigation of the Diffusion Characteristics of Supersonic Streams Composed Mainly of Boundary Layers

J. W. Cnossen* and R. L. O'Brien†
United Aircraft Corporation, East Hartford, Conn.

The diffusion characteristics of a supersonic stream composed primarily of boundary-layer flow were investigated using an annular supersonic wind tunnel discharging into an annular diffusion system representative of the surfaces near the throat region of an axisymmetric hypersonic inlet. Tests were conducted over a range of freestream Mach numbers of 2 to 5. At each test Mach number, the boundary layer approaching the diffuser was varied by changing the length of the constant area section upstream of the models. Data for diffusion system pressure recovery, static pressure distributions, and velocity profiles were obtained at each test Mach number for a range of area contraction ratios, convergence angles, and Reynolds numbers. An analytical method for predicting the performance of the supersonic boundary-layer diffusion system was developed on the basis of an experimental correlation of the minimum throat Mach number with an average flow distortion parameter. Both the analytical and experimental results indicate that the maximum pressure recovery of a supersonic boundary-layer diffusion system is obtained with a convergent section having a low convergence angle, between 3° and 6°. This analysis, which was developed for duct flows composed entirely of boundary layers, can also be employed to analyze duct flows having an inviscid core. The application of this method in calculating the performance of a hypersonic inlet is illustrated by means of examples.

Nomenclature

A = flow area
C_D = drag coefficient
C_f = skin-friction coefficient
CR = contraction ratio, A_1/A_2
D = distortion index, Eq. (1)
f = kinetic stream thrust, ρu^2
h = annular passage height
K = rate constant, Eq. (11)
L = axial distance from nozzle exit station
l = axial distance
l_T = throat length
M = Mach number
$\bar{M}$ = area average stream-thrust Mach number
$\mathring{m}$ = mass flow function, $g[\gamma/\Re]^{1/2} M\{1 + [(\gamma - 1)/2]M^2\}^{1/2}$
$\bar{m}$ = mass flow function, $P_S/P_T(\mathring{m})$
P_P = pitot pressure
P_R = total pressure recovery
P_S = static pressure
$\bar{P}_S$ = average static pressure
P_{S_m} = mean static pressure in throat
P_T = stagnation pressure
R = radius measured from model axis to outer wall of annular passage
Re = Reynolds number
Re_h = Reynolds number based on passage height
$\Re$ = gas constant for air
S = wetted area
T_S = static temperature
u = velocity
W_R = relative weight flow
x = axial distance from leading edge compression surface
Y = distance normal to surface
β = compression surface angle
γ = ratio of specific heats
δ = flow deflection angle
η_{sub} = subsonic diffuser efficiency; see Eq. (17)
θ = boundary-layer momentum thickness
ρ = density
ϕ = stream-thrust ratio, $\dfrac{1 + \gamma M^2}{M[2(\gamma + 1) \times \{1 + [(\gamma - 1)/2]M^2\}]^{1/2}}$

Subscripts

a = conditions in upper portion of step profile
av = average
b = conditions in lower portion of step profile
max = maximum
m = conditions at end of convergent section
n = conditions in nth region in convergent section
0 = conditions at nozzle exit
1 = conditions at beginning of convergent section
2 = conditions at beginning of throat
3 = conditions at end of throat
4 = conditions at end of subsonic diffuser
I = conditions upstream of shock
II = conditions downstream of shock
III = conditions at end of constant-area section

Superscripts

$(\bar{\ })$ = average conditions
$(')$ = ideal conditions

Introduction

TESTS of hypersonic inlets at Mach numbers above 5.0 have shown that the performance is extremely sensitive to variations in the boundary-layer characteristics.[1,2] At freestream Mach numbers above approximately 5.0, the boundary layer on the surfaces of internal compression inlets can extend completely across the duct upstream of the inlet throat, and the efficiency of the compression of this boundary-layer flow has a large influence on inlet performance. Boundary-layer calculation procedures such as those presented in Refs. 3 and 4 can be employed to predict the boundary-layer characteristics upstream of the station where the boundary layer extends across the duct, and normal shock and subsonic diffusion losses can be evaluated from information presented in Ref. 5. However, there is no known theory and very little data relative to the characteristics of fully developed pipe-flow boundary layers in a supersonic compression region.

The object of the present investigation was to obtain detailed information concerning the diffusion characteristics

Presented as Preprint 64-245 at the 1st AIAA Annual Meeting, Washington, D. C., June 29–July 2, 1964; revision received June 28, 1965.

* Research Engineer, Research Laboratories. Member AIAA.
† Supervisor, Air-Breathing Propulsion, Research Laboratories. Member AIAA.

TEST CONDITIONS		
M_0	LOW Re_{h_0}	HIGH Re_{h_0}
2.2	0.15 x 10^6	0.49 x 10^6
3.5	0.24 x 10^6	0.72 x 10^6
5.0	0.14 x 10^6	0.37 x 10^6

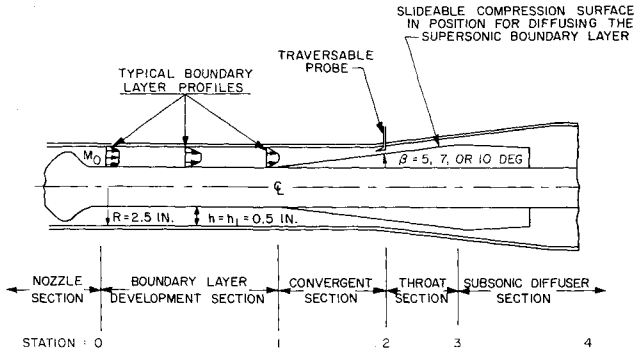

Fig. 1 Schematic drawing of boundary-layer diffusion model.

of supersonic duct flow composed mainly of boundary layer in order to provide a more rational basis for the design of hypersonic inlets having internal compression. A summary of some of the data obtained, a brief description of the analysis, and examples illustrating the use of this analysis in calculating the performance of hypersonic inlets are presented in Ref. 6.

Experimental Investigation

Description of Models

The geometry of the models tested was selected to simulate the convergent section just upstream of the throat of an axisymmetric hypersonic internal or external-plus-internal compression inlet. The boundary layer upstream of the diffuser model was allowed to develop in a long constant-area annular section into which the flow from the supersonic nozzle is discharged as shown in Fig. 1. The shape of the profile entering the diffuser could be varied by adding or removing segments of the annular passage, thereby changing the length of the constant-area section.

The convergent section of the diffuser, which simulated the supersonic compression surfaces of an inlet, was created by sliding a conical compression surface into the aft end of the annular passage, as shown in Fig. 1. Three models having conical convergent sections of 5°, 7°, and 10° were tested. Downstream of the supersonic diffuser a throat section having a total divergence angle of approximately 2° was formed by diverging the outer walls of the tunnel. Such a throat divergence was found to be necessary in previous tests reported in Ref. 7. The flow then passed through a subsonic diffuser having a total divergence angle of 7° and was then dumped into a large-diameter pipe.

Internal Aerodynamics

Tests were conducted at nominal Mach numbers at the nozzle exit of 2.2, 3.5, and 5.0 with either 5°, 7°, or 10° compression-surface models located in the boundary-layer development section. At each Mach number, tests were conducted at two Reynolds numbers with the models located at three or more stations ranging from 14 to 38 passage heights downstream from the nozzle exit. For each Mach number and Reynolds number, one of these stations was located upstream of pipe flow, one near the beginning of pipe flow, and one in the region of well-established pipe flow. For each test condition, data were obtained for a range of model contraction ratios. The contraction ratio of the model is defined as the ratio of the flow area at the start of the convergent section, A_1 to the flow area at the start of the throat section A_2.

Static pressure distributions on both the inner and outer walls of the convergent and throat sections of the supersonic diffuser were obtained at freestream Mach numbers 2.2, 3.5, and 5.0 with the compression surface located at the position for maximum contraction ratio and with the shock located as close to the throat as possible, i.e., further throttling would force the shock upstream of the convergent section. A typical static pressure distribution measured at a nominal Mach number of 5.0 (average Mach number of 3.75) is shown in the top portion of Fig. 2. The static pressure distribution shown here was measured on the outer wall of the tunnel. The theoretical wall static pressure distribution corresponding to these test conditions is also shown in this figure. This theoretical distribution was determined from the inviscid oblique shock relationships using the average Mach number at the entrance to the convergent section and a deflection angle equal to the convergent section wall angle. Pitot pressure profiles obtained at various stations in the convergent section are shown in the lower portion of Fig. 2.

Wall static pressure distributions were measured on both the inner and outer walls of the flow passages for various model locations and Mach numbers. These pressure distributions were in general agreement with the distribution just discussed. The theoretical distributions were calculated for all of the configurations tested. The agreement between theory and experiment in all cases is comparable to that shown in Fig. 2. The experimental static pressure distributions in the throat section indicated that the throat was of insufficient length to contain the complete normal shock static pressure rise. From data in Ref. 8 on the throat length required to contain the normal shock static pressure rise in an annular passage and from data in Ref. 5 on the effect of insufficient throat length on the over-all pressure

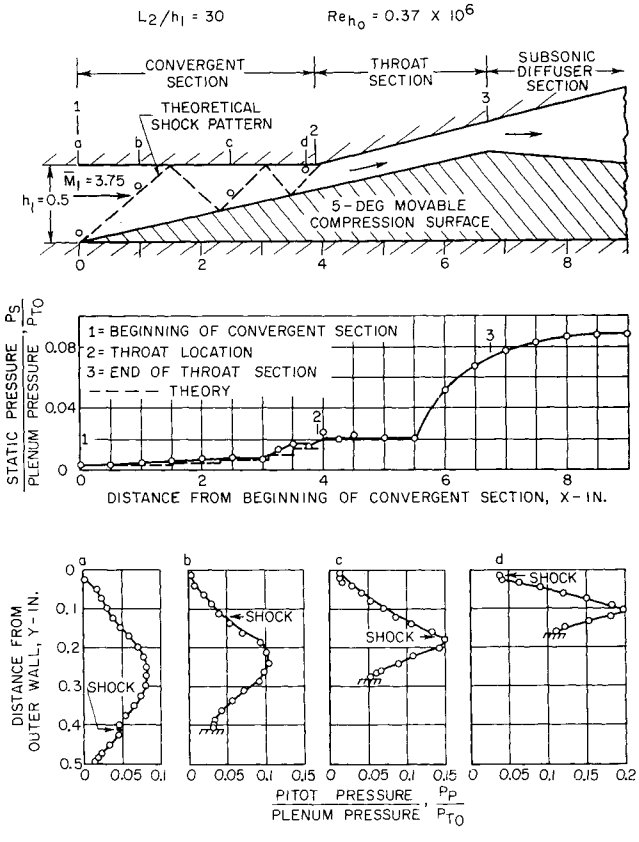

Fig. 2 Typical flow pattern, static pressure distribution, and pitot profiles.

recovery of a supersonic diffuser system, it was estimated that the loss in pressure recovery due to insufficient throat length was approximately 1 to 5% of the theoretical pressure recovery, with the greater losses occurring at the higher test Mach numbers.

The upstream pitot pressure profiles just presented show small discontinuities, indicating the shock locations; the downstream profiles do not show these discontinuities, indicating that the shocks were no longer discreet waves. These data, which are typical of those obtained at other Mach numbers and upstream flow conditions, show an increase in the maximum pitot pressure along the duct because of increased compression and a tendency toward a triangular profile at the end of the convergent section. All of the profile data were analyzed, and the results were employed in the theoretical investigation to be described subsequently. The theoretical inviscid shock pattern in the convergent section and an estimate of the location of the shocks obtained from the profile data are also given. The agreement between the inviscid wave pattern and the data is very good near the upstream end of the convergent section.

Pressure Recovery

A summary of the maximum model pressure recoveries and contraction ratios is presented in Fig. 3 as a function of the average Mach number at the beginning of the convergent section. The data for the 5° and 10° models fall along two different lines, with the 5° models having the higher pressure recoveries and contraction ratios. The data for the 5° model, which were obtained with some inviscid-core flow entering the convergent section ($L_2/h_1 = 22$), are slightly higher than the line faired through data points obtained with pipe-flow profile ($L_2/h_1 = 30$ and 38). This can be attributed to the less distorted profile at the beginning of the convergent section. Also shown in this figure is the pressure recovery obtained with no area contraction ($CR = 1.0$) to indicate the degree of improved performance obtained with the diffusion model. This curve is significantly lower than the ideal normal shock recovery and shows the large losses that would be incurred by terminating the internal contraction region of an inlet at the station where fully developed pipe flow is established. For the low Mach number tests, the maximum pressure recoveries obtained were slightly less than the ideal normal shock recovery and slightly greater than the pressure recovery for $CR = 1.0$, whereas for the high Mach number tests the maximum pressure recoveries are 50 to 100% greater than the ideal normal shock pressure recovery and 100 to 300% greater than the $CR = 1.0$ value. Thus, for a high Mach number inlet, it is extremely important to continue supersonic diffusion past the point where pipe flow is established. Similar data obtained at lower Reynolds numbers show the same characteristics; however, lower pressure recoveries and contraction ratios were obtained.

Theoretical Investigation

The theoretical analysis of the supersonic boundary-layer diffusion process was formulated to be compatible with the type of data obtained from the experimental investigation. Consequently, an attempt was made to provide a theory that takes into consideration the limitations imposed by profile data obtained with a pitot probe in a compression region having shock waves and a nonuniform static pressure distribution across the duct.

Although the wall static pressure was measured, the static pressure profiles across the duct could not be measured accurately with a static pressure probe because of the nonuniform flow direction and the curvature of the streamlines. Thus standard boundary-layer calculation procedures, which would require this nonuniform static pressure profile to be

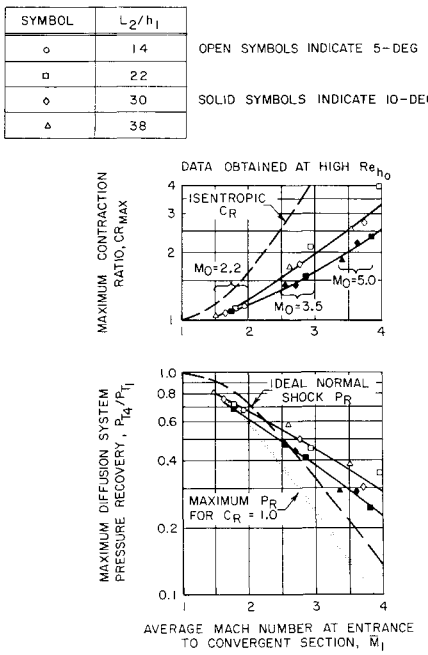

Fig. 3 Variation of maximum contraction ratio and maximum pressure recovery with average Mach number.

estimated, could result in large errors in the standard boundary-layer integral parameters (momentum thickness and displacement thickness), which are sensitive to the shape of the assumed static pressure profile. Therefore, the analysis of the boundary-layer diffusion process was based on a parameter that is insensitive to the assumed static pressure and determined primarily from the pitot pressure profile. Such a property is exhibited by the kinetic stream thrust $f = \rho u^2$; calculations at a Mach number of 3.0 show that a 50% increase in the assumed static pressure results in only a 2.02% decrease in kinetic stream thrust for a given value of the pitot pressure. Hence it is possible to determine the stream-thrust profile from the experimental pitot pressure profiles with very little error due to the assumed nonuniform static pressure profile at that station. The parameters used to define the flow conditions at a given station were, therefore, derived from the stream-thrust profile. The average Mach number used in the analysis $\bar{M}$ was defined from the area average of the stream thrust, and the distortion index D was defined by the following expression:

$$D = (\int_A |f - f_{av}| dA)/(A \cdot f_{av}) \quad (1)$$

where

$$f_{av} = \int_A f dA/A = \bar{P}_S \gamma \bar{M}^2 \quad (2)$$

The experimentally determined values of the distortion index for profiles obtained in the constant-area boundary-layer development section are presented on the left-hand side of Fig. 4 as a function of the average Mach number. The distortion indices for $\frac{1}{7}$ and $\frac{1}{9}$ power law profiles are also shown in this figure. The data in the fully developed pipe-flow region are in general agreement with the distortion index for a $\frac{1}{9}$ power profile. Consequently, the value of D for a $\frac{1}{9}$ power profile $D_{1/9}$ was used in the present analysis to represent the equilibrium value for fully developed pipe flow.

The experimental values of the distortion index for profiles obtained at the end of the convergent section or entrance to the throat section are presented on the right-hand side of Fig. 4. The data scattered about the faired curve with an rms deviation of 0.033. There was no significant trend with Reynolds number, length of constant-area passage, or compression surface geometry. Consequently, this single faired curve was used to define the maximum distortion that

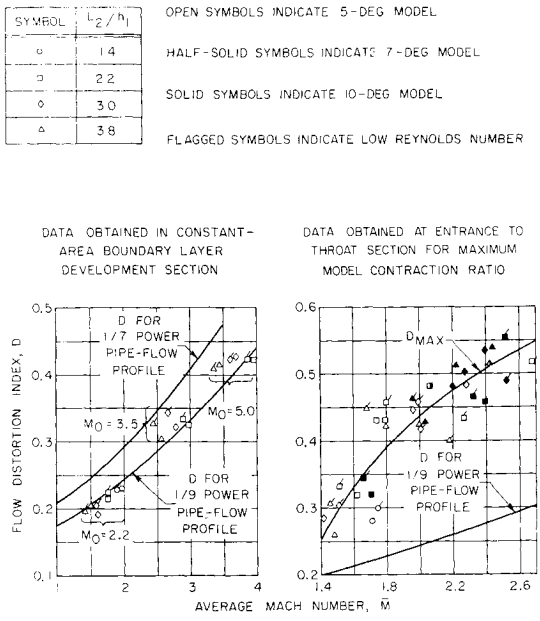

Fig. 4 Variation of distortion index with average Mach number.

could be tolerated prior to flow breakdown in the convergent section.

The method of analysis used to compute the maximum contraction ratio of the convergent section consisted of calculating the variation of the distortion index and average total pressure with the average Mach number in the convergent section and terminating the calculation when the value of the distortion index crossed the empirically determined maximum value, as determined by the faired curve in Fig. 4. The total pressure losses across the normal shock in the throat region were computed in a manner that included the effects of throat friction and throat divergence, and the total pressure losses in the subsonic diffuser were computed by assuming a conventional subsonic diffuser efficiency. A detailed derivation of the theoretical analysis is presented in the following paragraphs.

Convergent Section Analysis

In the convergent section, the flow is decelerated by reflected oblique shocks and by wall friction. The shock losses in the convergent section are further complicated by the existence of a nonuniform flow upstream of the waves which introduces additional losses due to mixing. A schematic diagram of the idealized flow in the convergent section is shown in Fig. 5. In the calculation procedure, the idealized flow is replaced by a pseudo-one-dimensional flow model also shown in Fig. 5. In this model, the flow properties change discontinuously across shocks. As shown in the lower portion of this figure, the Mach number is decreased discontinuously across the waves in the convergent section and is further decreased by wall friction in the constant-area sections. The distortion index is increased by the shock waves but decreased in the constant-area sections between the waves.

Total pressure and distortion index changes across shock waves

For this model, the flow conditions (average Mach number, average total pressure, and distortion index upstream of the shock at station I) are known either from the initial conditions at the beginning of the convergent section or from the conditions at the end of the preceding region. The flow properties downstream of the shock (station II) were computed from relationships developed for the change of a step profile across the discontinuous static pressure rise created by an oblique shock. The step profile was defined to have the same average stream thrust, average Mach number, and distortion index as the actual profile. A sketch of the actual and step profiles employed in this analysis is presented in Fig. 6. The average stream thrust, average Mach number, and distortion index are defined as follows for the two profiles:

$$\text{actual profile} \qquad \text{step profile}$$

$$f_{av} = \frac{\int_A f\,dA}{A} = \frac{f_a A_a + f_b A_b}{A_a + A_b} \tag{3}$$

$$\bar{M}^2 = \frac{\int_A M^2\,dA}{A} = \frac{M_a^2 A_a + M_b^2 A_b}{A_a + A_b} \tag{4}$$

$$D = \frac{\int_A |f - f_{av}|\,dA}{f_{av} A} = \frac{(f_a - f_{av})A_a + (f_{av} - f_b)A_b}{f_{av}(A_a + A_b)} \tag{5}$$

Since the average stream thrust is the area average of the stream thrust, $(f_a - f_{av})\,A_a = (f_{av} - f_b)A_b$, for the step profile, and Eq. (5) reduces to

$$D = \left[1 - \frac{M_b^2}{\bar{M}^2}\right] \cdot \frac{2}{1 + (A_a/A_b)} \tag{6}$$

Equation (6) therefore relates the Mach number M_b and area ratio A_a/A_b of the step profile to the average Mach number $\bar{M}$ and distortion index D of the actual profile.

To obtain the flow conditions in the step profile downstream of the shock wave, each part of the step was passed through an oblique shock having the same static pressure rise, and the mass flow in each part of the step was conserved. The pressure ratio across the wave was determined from oblique shock relationships for the average upstream Mach number and a flow deflection angle equal to the duct convergence angle. The flow conditions downstream of the wave for each portion of the step were determined from oblique shock tables for a wave having the same static pressure ratio as defined previously. It should be noted that, since the mass flow was conserved in each part of the step, the area ratio A_a/A_b will change across the wave. From the values of the area ratio and the Mach numbers downstream of the wave, the distortion index D can be determined from Eq. (6). The total pressure ratio across the wave may be obtained by applying the conditions of continuity to the average flow conditions on either side of the wave. This yields

$$\frac{P_{T_{II}}}{P_{T_I}} = \frac{\bar{m}_{avI}}{\bar{m}_{avII}} \cdot \frac{A_I}{A_{II}} = \left(\frac{\bar{m}_{bI}}{\bar{m}_{bII}}\right) \cdot \left(\frac{\bar{m}_{av}}{\bar{m}_b}\right)_I \cdot \left(\frac{\bar{m}_b}{\bar{m}_{av}}\right)_{II} \cdot \frac{(A_a + A_b)_I}{(A_a + A_b)_{II}} \tag{7}$$

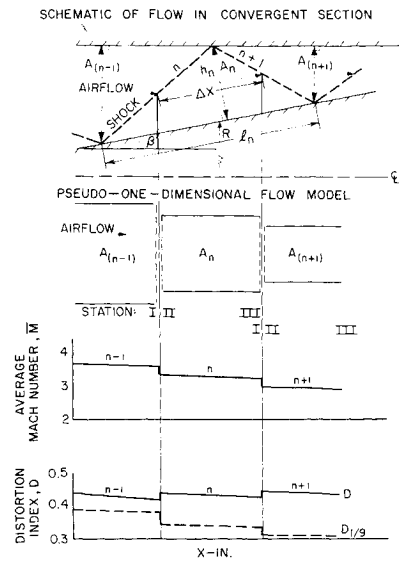

Fig. 5 Flow model for theoretical calculation.

where $\bar{m}$ is a mass flow function of local Mach number and is tabulated in Ref. 9. If the condition of conservation is applied now to the flow in the lower portion of the step profile, the following relation is obtained:

$$\frac{\bar{m}_{b\mathrm{I}}}{\bar{m}_{b\mathrm{II}}} = \left(\frac{P_{T\mathrm{II}}}{P_{T\mathrm{I}}}\right)_b \frac{A_{b\mathrm{II}}}{A_{b\mathrm{I}}} \tag{8}$$

Substituting Eq. (8) into Eq. (7) then yields

$$\frac{P_{T\mathrm{II}}}{P_{T\mathrm{I}}} = \left(\frac{P_{T\mathrm{II}}}{P_{T\mathrm{I}}}\right)_b \cdot \left(\frac{\bar{m}_{\mathrm{av}}}{\bar{m}_b}\right)_{\mathrm{I}} \cdot \left(\frac{\bar{m}_b}{\bar{m}_{\mathrm{av}}}\right)_{\mathrm{II}} \cdot \left[\frac{1 + (A_a/A_b)_{\mathrm{I}}}{1 + (A_a/A_b)_{\mathrm{II}}}\right] \tag{9}$$

The area ratio $(A_a/A_b)_{\mathrm{II}}$ may be evaluated by applying the condition of continuity to the flow in each part of the step individually and noting that the static pressure is constant across the profile. This leads to the following relationship:

$$\left(\frac{A_a}{A_b}\right)_{\mathrm{II}} = \left(\frac{\mathring{m}_a}{\mathring{m}_b}\right)_{\mathrm{I}} \cdot \left(\frac{\mathring{m}_b}{\mathring{m}_a}\right)_{\mathrm{II}} \cdot \left(\frac{A_a}{A_b}\right)_{\mathrm{I}} \tag{10}$$

where $\mathring{m}$ is another mass flow function tabulated in Ref. 9. Substituting this result into Eq. (9) yields

$$\frac{P_{T\mathrm{II}}}{P_{T\mathrm{I}}} = \left(\frac{P_{T\mathrm{II}}}{P_{T\mathrm{I}}}\right)_b \cdot \left(\frac{\bar{m}_{\mathrm{av}}}{\bar{m}_b}\right)_{\mathrm{I}} \cdot \left(\frac{\bar{m}_b}{\bar{m}_{\mathrm{av}}}\right)_{\mathrm{II}} \times \left[\frac{1 + (A_a/A_b)_{\mathrm{I}}}{1 + (A_a/A_b)_{\mathrm{I}} \cdot (\mathring{m}_a/\mathring{m}_b)_{\mathrm{I}} \cdot (\mathring{m}_b/\mathring{m}_a)_{\mathrm{II}}}\right] \tag{11}$$

Calculations of the total pressure and distortion index of a step profile downstream of a shock wave for given upstream conditions indicate that the changes in these parameters are relatively insensitive to the value of the area ratio (A_a/A_b) upstream of the wave. For simplicity, this ratio was assumed to be equal to 1.0. Equation (11) is then reduced to

$$\frac{P_{T\mathrm{II}}}{P_{T\mathrm{I}}} = \left(\frac{P_{T\mathrm{II}}}{P_{T\mathrm{I}}}\right)_b \cdot \left[\frac{2(\bar{m}_{\mathrm{av}}/\bar{m}_b)_{\mathrm{I}}(\bar{m}_b/\bar{m}_{\mathrm{av}})_{\mathrm{II}}}{1 + (\mathring{m}_a/\mathring{m}_b)_{\mathrm{I}}(\mathring{m}_b/\mathring{m}_a)_{\mathrm{II}}}\right] \tag{12}$$

The results of this calculation procedure are presented in Fig. 7 for shock deflection angles of 5° and 10°. The top half of this figure shows the variation of the distortion index downstream of the wave D_{II} as a function of the average Mach number $\bar{M}$ and initial distortion index D_{I}. As expected, a D_{I} of zero results in a D_{II} of zero, and a D_{I} greater than zero results in $D_{\mathrm{II}} > D_{\mathrm{I}}$. The increase in the distortion index across the waves also becomes larger as the average Mach number upstream of the wave is decreased. The total pressure ratios are presented in the lower half of this figure. The curve for D_{I} equal to zero represents the ideal value for uniform upstream flow. As the initial distortion is increased, the total pressure losses across the shock increase.

Total pressure and distortion index changes in constant-area sections

The analysis of the effects of wall friction on the flow in the constant-area duct between the waves (see Fig. 5) was

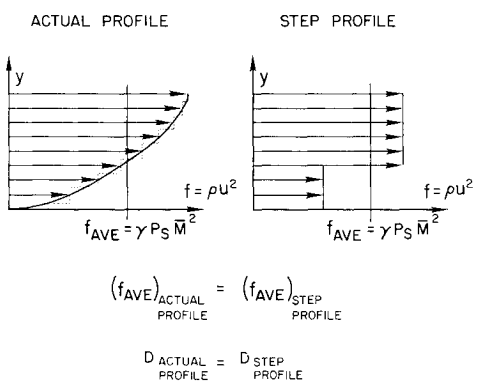

Fig. 6 Sketch of velocity profiles employed in analysis.

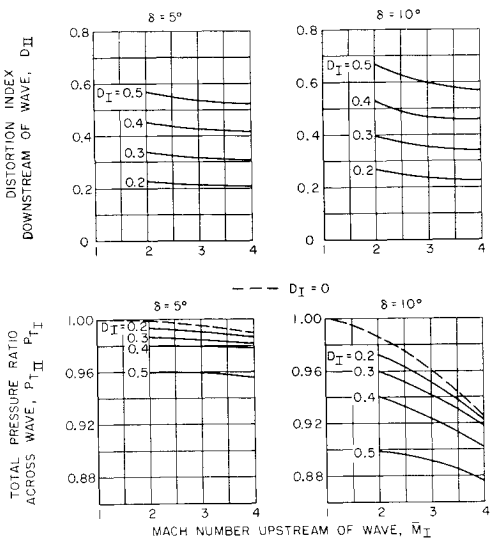

Fig. 7 Change in average flow properties of a step profile across an oblique shock wave.

formulated in terms of incremental changes in the average properties along this flow channel. From the equations of continuity, momentum, energy, and state, the following equation for the change in flow velocity may be derived:

$$du/u = [-\gamma C_f/(1 - 1/M^2)]\, d\,(x/h) \tag{13}$$

For most cases, the change in $(\gamma C_f)/(1 - 1/M^2)$ between stations II and III is small, and this equation may be written in a more convenient form by replacing the differential changes in velocity and distance with their corresponding incremental values. A value of C_f of 0.001 (approximately half the flat-plate value) was used to account for the reduction in skin friction due to velocity profile distortion. The passage length Δx employed in Eq. (13) was evaluated to provide a surface area in the one-dimensional model equal to the surface area between shocks, as indicated in Fig. 5. For a thin annular duct,

$$\Delta x/h_n = \tfrac{1}{2}(ln/h_n) \tag{14}$$

The change in average Mach number may be evaluated from the change in velocity given by Eq. (13), and the loss in total pressure may be evaluated by equating mass flow.

The change in the distortion index in the constant-area duct was evaluated by the following equation:

$$dD_{\mathrm{II}\to\mathrm{III}} = -K(D_{\mathrm{II}} - D_{1/9})d(x/h) \tag{15}$$

The rate constant K was evaluated by employing Eq. (15) to predict the start of pipe flow in a constant-area duct. The start of pipe flow was taken at the point where D is equal to the equilibrium value for pipe flow $D_{1/9}$. This calculation was performed for the cases for which data were obtained in this investigation, and comparison of the predicted and measured values of passage length at the start of pipe flow established the value of K as approximately 0.04. The rate constant K would be expected to be a function of both Mach number and Reynolds number, but, for the range of flow conditions covered in this investigation, no systematic variation of K with either Mach or Reynolds numbers could be observed.

Solution for the entire convergent section

To complete the analysis of the flow in the convergent section, the section is divided into m regions labeled in accordance with the number of oblique shock waves. In each region, the flow is treated by the pseudo-one-dimensional analysis, consisting of a shock followed by a constant-area

passage, as described in the preceding paragraphs. The conditions at the end of each constant-area passage, designated by III, become the initial conditions for each successive step of the calculation. The total pressure ratio along the convergent section is the cumulative product of the total pressure ratio for each region

$$\frac{P_{T_m}}{P_{T_1}} = \prod_{n=1}^{m} \frac{P_{T_{III}}}{P_{T_1}}$$

and the contraction ratio along the convergent section is given by

$$CR = A_1/A_m = (\bar{m}_m/\bar{m}_1)(P_{T_m}/P_{T_1}) \tag{16}$$

Throat Analysis

The total pressure losses in the throat section include the friction and throat divergence losses. The momentum equation in the throat region may be written as

$$\underset{\text{exit station momentum}}{P_{S_3}A_3(1+\gamma\bar{M}_3^2)} = \underset{\text{entrance station momentum}}{P_{S_2}A_2(1+\gamma\bar{M}_2^2)} - C_f(\gamma/2)P_{S_2}\bar{M}_2^2S + \underset{\text{wall force}}{P_{S_m}(A_3-A_2)} \tag{17}$$

$$\underset{\text{friction force}}{}$$

The ratio of the momentum equation to the continuity equation across the throat is proportional to the stream-thrust ratio ϕ. Thus,

$$\phi_3 = g\left[\frac{\gamma}{2(\gamma+1)\mathfrak{R}}\right]^{1/2}\left(\frac{1+\gamma\bar{M}_3^2}{\mathring{m}}\right) = 0.41942\left[1+\gamma\bar{M}_2^2\left(1-C_f\frac{l_T}{h}\right)+\frac{P_{S_m}}{P_{S_2}}\left(\frac{A_3}{A_2}-1\right)\right]\Big/\mathring{m}_2 \tag{18}$$

where, for air,

$$q\,[\gamma/2(\gamma+1)\mathfrak{R}^{1/2}] = 0.41942$$

For the experimental tests, the throat was found to be of insufficient length to contain the normal shock, and it was found that the ratio of the mean static pressure in the throat to the static pressure at the throat entrance could be as expressed as

$$P_{S_m}/P_{S_2} = 1 + \tfrac{1}{3}[(P_{S_3}'/P_{S_2}) - 1] \tag{19}$$

where P_{S_3}' is the ideal static pressure downstream of the normal shock in the throat. Since l_T/h and A_3/A_2 are determined by the model geometry, the average Mach number

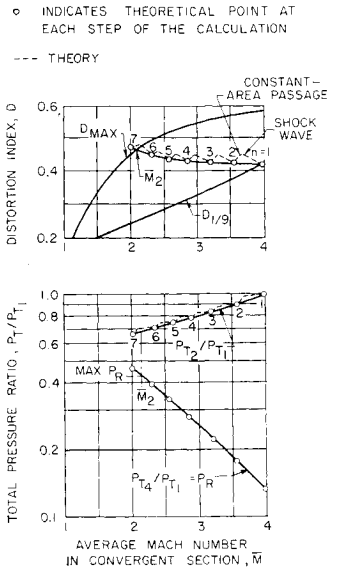

Fig. 8 Example showing variation of flow parameters with average Mach number in convergent section.

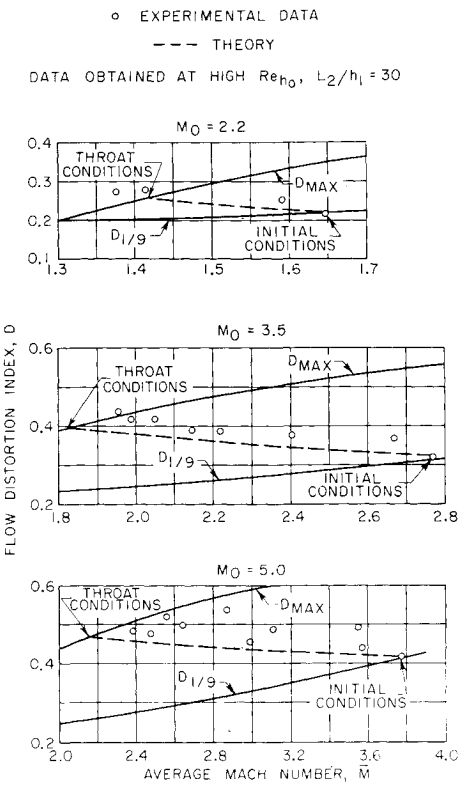

Fig. 9 Variation of distortion index with average Mach number in convergent section.

at the throat exit may be determined. The total pressure ratio across the throat may then be determined from the continuity equation in the form

$$P_{T_3}/P_{T_2} = (\bar{m}_2/\bar{m}_3)\cdot(A_2/A_3) \tag{20}$$

Subsonic Diffuser Analysis

The losses in the subsonic diffuser were based on a conventional subsonic diffuser efficiency, which may be written as

$$\eta_{\text{sub}} = (P_{S_4}-P_{S_3})/[(P_{T_3}-P_{S_3}) - (P_{T_4}-P_{S_4})] \tag{21}$$

Noting that, for low exit Mach number, $P_{T_4} \approx P_{S_4}$, Eq. (21) may be rearranged to become

$$P_{T_4}/P_{T_3} = \eta_{\text{sub}} + (P_{S_3}/P_{T_3})(1-\eta_{\text{sub}}) \tag{22}$$

The value of η_{sub} used in the model analysis was 0.75, and the value used for the hypothetical inlet calculations was 0.85.

Diffusion System Pressure Recovery

The total pressure recovery of the entire system is the cumulative product of the pressure ratios across each section and may be computed as follows:

$$P_R = \frac{P_{T_4}}{P_{T_1}} = \left(\frac{P_{T_m}}{P_{T_1}}\right)\left(\frac{P_{T_3}}{P_{T_2}}\right)\left(\frac{P_{T_4}}{P_{T_3}}\right) \tag{23}$$

The results of a representative calculation are shown in Fig. 8, which represents the variation of the distortion index and total pressure recovery with average Mach number for a complete calculation through the convergent section. The dashed, saw-tooth curve in the upper half of the figure shows the detailed path of the calculation of the distortion index. The distortion index increases and Mach number decreases across the shocks, whereas the distortion index decreases and the Mach number decreases in the constant-area passages. The solid line through the end points of each complete step (shock plus constant-area passage) in the calcula-

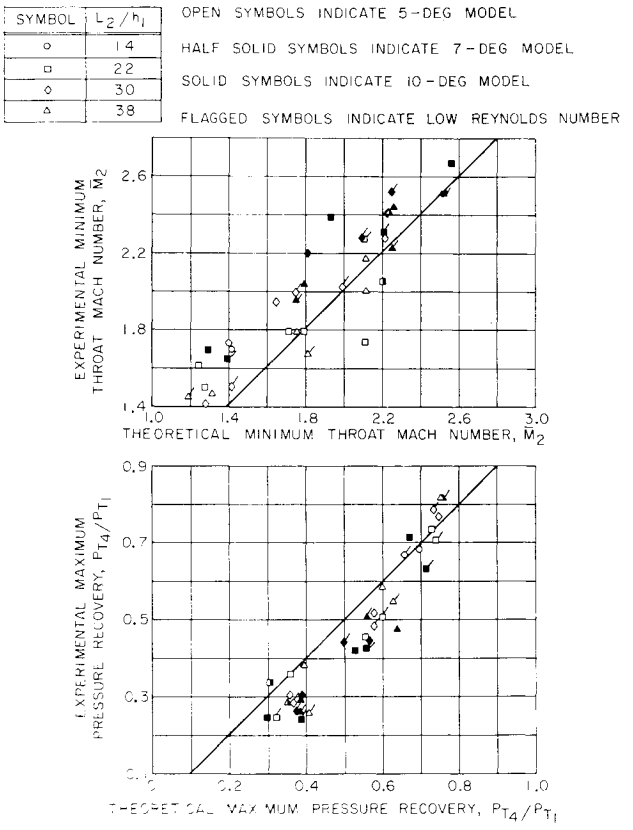

Fig. 10 Comparison of theoretical and experimental performance.

tion represents the true path of the distortion index. The throat Mach number was determined from the intersection of the true path of the distortion index and the maximum value of the distortion index. The lower portion of Fig. 8 shows the variation of the average total pressure in the convergent section and the total pressure recovery that would be realized if the convergent section were terminated at a station having an average Mach number given by the horizontal ordinate.

Correlation of Theoretical Analysis with Experimental Data

Theoretical calculations were made for all of the test conditions reported in the experimental section, with initial conditions determined from the experimental data. Some typical examples of the theoretical variation of the distortion index with average Mach number along the convergent sections are compared in Fig. 9 with the values obtained from experimentally measured profile data. These correlations were obtained with the compression surface located near the beginning of pipe flow; however, all of the theoretical results are in general agreement with the experimental data.

Correlations of experimental data from all test conditions with theoretical values of the minimum throat Mach number and maximum pressure recovery are presented in Fig. 10. General agreement of theory with experimental data is noted; the scatter is attributed to the accuracy of the experimental parameters plotted and to the selection of a unique curve for defining the distortion index (Fig. 4).

Figure 11 shows the effect of duct convergence angle on diffuser system performance for nominal Mach numbers of 3.5 and 5.0. The theoretical and experimental results show the same trends and approximate values; the optimum convergence angle was approximately 5°. For lower angles larger friction losses were incurred, and for higher angles the oblique shock losses were increased. Therefore, it can be concluded that, for high Mach number inlets with a region of pipe flow upstream of the throat, the optimum convergence angle just upstream of the throat should be approximately 5°.

Application of Theory to Hypersonic Inlet Performance

Theoretical Calculation of Mach 8 Inlet Performance

The theoretical analysis derived in the preceding sections can also be employed to compute the approximate performance of supersonic or hypersonic inlets by simply letting the initial value of the distortion index be zero, since the flow upstream of the first shock is the uniform freestream. The entire calculation procedure is followed without modification; however, for the inlet performance presented, throat-friction and throat-divergence losses were neglected. The theoretical performance of axisymmetric, external-plus-internal compression inlets having 5° or 10° compression surfaces and a design Mach number of 8.0 is presented in Fig. 12. Although both inlets would have approximately the same minimum throat Mach number, the 10° configuration attained a higher pressure recovery because the long 5° configuration had greater total pressure losses in the convergent section caused by wall friction.

In the preceding section, it was concluded that the optimum convergence angle in the pipe-flow section of an inlet is approximately 5°. However, this conclusion does not apply to the upstream portion, where there is an inviscid core. Consequently, a third inlet configuration was analyzed to verify this conclusion. For this configuration the upstream portion (core-flow region) of the inlet had a 10° convergence angle, and the downstream portion of the inlet (pipe-flow region) had a 5° convergence angle. The results of this calculation are presented in the upper half of Fig. 13 for design Mach numbers of 5.0, 8.0, and 10. This third configuration produced a higher pressure recovery than an inlet with either 5° or 10° convergence angle for this range of Mach numbers. It should be remembered that these results are from approximate calculations that neglected throat-friction and divergence losses and subsonic diffusion losses.

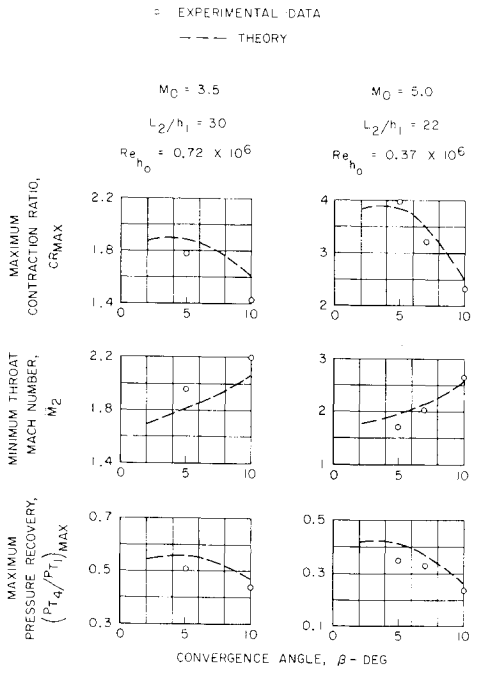

Fig. 11 Effect of convergence angle on diffusion system performance.

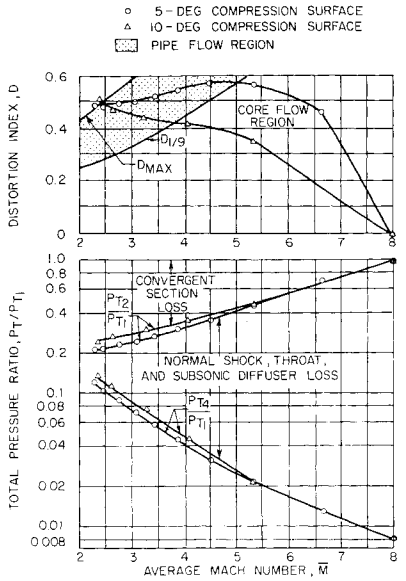

Fig. 12 Results of theoretical calculation of Mach 8 inlet performance.

Calculations were also performed to determine the off-design performance of the Mach 8.0 inlet with a 10° convergence angle for Mach numbers from 2.0 to 10.0. The results of this analysis are presented in the lower half of Fig. 13, along with the design point performance of a 10° inlet for comparison. For this calculation, the throat area was assumed to vary linearly with centerbody position, and so the inlet throat area varied from approximately 30% of the capture area at Mach 2.0 to 4.5% of the capture area at Mach 8.0. Below Mach 8.0, airflow was spilled externally behind the conical shock. At Mach numbers above 8.0, the inlet would operate with the conical shock intersecting the cowl surface to the rear of the cowl lip. The off-design pressure recovery is less than the design point pressure recovery for both cases. The performance of a Mach 8.0 inlet operating at Mach numbers less than 8.0 is less than the design point performance because the ratio of the wetted surface area to the capture area is larger for the Mach 8.0 inlet than it is for the design point inlets. In addition, the relatively long compression surface on which boundary layer develops results in considerable distortion of the flow upstream of the convergent section. The effect of the relatively thick boundary layer entering the convergent section at off-design Mach numbers could be reduced by bleeding some of the boundary layer from the compression surface upstream of interaction of the shock from the cowl lip. Thus, the flow entering the convergent section would be more uniform and would have less distortion than it would without bleed.

The results presented in this paper show that the analysis developed herein can be employed to determine the performance of the pipe-flow section of an internal contraction inlet and to estimate the performance of hypersonic air induction systems. The results of the theoretical calculations show that the optimum convergence angle in the pipe-flow section of an inlet is approximately 5°.

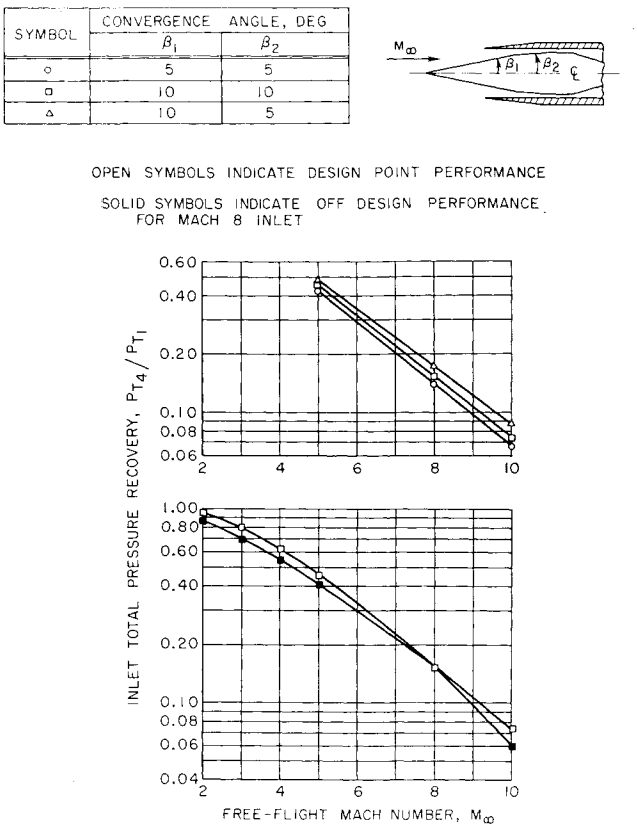

Fig. 13 Variation of theoretical inlet performance with freestream Mach number.

References

[1] McLafferty, G. H., "Hypersonic inlet studies at UAC Research Laboratories," United Aircraft Corp., Research Labs. Rept. M-2000-113 (December 1959).

[2] Kepler, C. E., Cnossen, J. W., and Demarest, P. E., "Hypersonic inlet investigations including tests to Mach 8.7 and theoretical analyses to Mach 15," Aeronautical Systems Div. TR 61-137 (June 1961); confidential (unclassified title), no classified material extracted from this report.

[3] McLafferty, G. H. and Barber, R. E., "Turbulent boundary layer characteristics in supersonic streams having adverse pressure gradients," United Aircraft Corp., Research Labs. Rept. R-1285-11 (September 1959).

[4] Kepler, C. E. and O'Brien, R. L., "Supersonic turbulent boundary layer growth over cooled walls in adverse pressure gradients," Aeronautical Systems Div. Tech. Doc. Rept. ASD TDR 62-87 (October 1962).

[5] McLafferty, G. H., Krasnoff, E. L., Ranard, E. D., Rose, W. G., and Vergara, R. D., "Investigation of turbojet inlet design parameters," United Aircraft Corp., Research Labs. Rept. R-0790-13 (December 1955).

[6] Cnossen, J. W. and O'Brien, R. L., "Investigation of the diffusion characteristics of supersonic streams composed mainly of boundary layers," Aeronautical Systems Div. Tech. Doc. Rept. ASD TDR 62-528 (October 1962).

[7] Cnossen, J. W., "Studies of boundary layer removal scoops for high-performance supersonic inlets," United Aircraft Corp., Research Labs. Rept. R-0955-21 (October 1957).

[8] Burr, J., "Characteristics of normal shock waves in annular passages," United Aircraft Corp., Research Labs. Rept. M-1266-3 (December 1959).

[9] Kennedy, E. C., Sonheim, D. W., and Barnes, A. M., "New Mach number flow tables for internal ramjet flow analysis," OAL Memo. 50, Ordnance Aerophysics Lab. (April 1952).